Acta Pharmaceutica Sinica B 2022;12(2):907–923

Chinese Pharmaceutical Association
Institute of Materia Medica, Chinese Academy of Medical Sciences

Acta Pharmaceutica Sinica B

www.elsevier.com/locate/apsb
www.sciencedirect.com

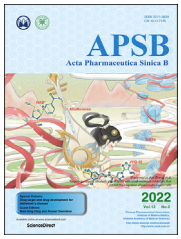

ORIGINAL ARTICLE

# Natural exosome-like nanovesicles from edible tea flowers suppress metastatic breast cancer *via* ROS generation and microbiota modulation

**Qiubing Chen[a,b,†], Qian Li[b,†], Yuqi Liang[a], Menghang Zu[a,b], Nanxi Chen[a], Brandon S.B. Canup[c], Liyong Luo[d], Chenhui Wang[e,*], Liang Zeng[d,*], Bo Xiao[a,b,*]**

[a]*State Key Laboratory of Silkworm Genome Biology, College of Sericulture, Textile, and Biomass Sciences, Southwest University, Chongqing 400715, China*
[b]*Chongqing Key Laboratory of Soft-Matter Material Chemistry and Function Manufacturing, School of Materials and Energy, Southwest University, Chongqing 400715, China*
[c]*Department of Chemistry, Center for Diagnostics and Therapeutics, Georgia State University, Atlanta, GA 30303, USA*
[d]*College of Food Science, Southwest University, Chongqing 400715, China*
[e]*Chongqing Key Laboratory of Natural Product Synthesis and Drug Research, School of Pharmaceutical Sciences, Chongqing University, Chongqing 401331, China*

Received 15 April 2021; received in revised form 22 June 2021; accepted 5 July 2021

*Abbreviations:* AF633, Alexa Fluor 633-labeled phalloidin; ALP, alkaline phosphatase; ALT, alanine aminotransferase; AST, aspartate aminotransferase; BUN, urea nitrogen; CDK, CYCLIN-dependent kinase; CRE, creatinine; DAF-FM DA, 4-amino-5-methylamino-2′,7′-difluorofluorescein diacetate; DAPI, 4′,6-diamidino-2-phenylindole; DCFH-DA, dichloro-dihydro-fluorescein diacetate; DHE, dihydroethidium; DiO, 3,3′-dioctadecyloxacarbocyanine perchlorate; DiR, 1,1′-dioctadecyl-3,3,3′′,3′-tetramethylindotricarbocyanine iodide; DGDG, digalactosyl diacylglycerols; DLS, dynamic light scattering; EC, epicatechin; ECG, epicatechin gallate; EGCG, epigallocatechin gallate; FBS, fetal bovine serum; GIT, gastrointestinal tract; H&E, Hematoxylin & Eosin; HPLC, high-performance liquid chromatography; LC–MS, liquid chromatography–mass spectrometry; MFI, mean fluorescence intensity; MGDG, monogalactosyl diacylglycerols; MTT, 3-(4,5-dimethylthiazol-2-yl)-2,5-diphenyltetrazolium bromide; NO, nitrogen monoxide; NPs, nanoparticles; OUT, operational taxonomic unit; PA, phosphatidic acids; PBS, phosphate-buffered saline; PC, phosphatidylcholines; PDI, polydispersity index; PE, phosphatidylethanolamines; PG, phosphatidylglycerol; PI, phosphatidylinositol; PLT, platelets; PMe, phosphatidylmethanol; PS, phosphatidylserine; RBC, red blood cell; RNS, reactive nitrogen species; ROS, reactive oxygen species; SA, superoxide anion; SQDG, sulphoquinovosyl diylyceride; TEM, transmission electron microscopy; TFENs, exosome-like NPs from tea flowers; TG, triglyceride; TUNEL, TdT-mediated dUTP Nick-end labeling; WBC, white blood cell.

*Corresponding authors. Tel./fax: +86 68254762 (Bo Xiao); +86 68250374 (Liang Zeng); +86 65678463 (Chenhui Wang)
E-mail addresses: wangchenhui@cqu.edu.cn (Chenhui Wang), zengliangbaby@126.com (Liang Zeng), bxiao@swu.edu.cn (Bo Xiao).
[†]These authors made equal contributions to this work.
Peer review under responsibility of Chinese Pharmaceutical Association and Institute of Materia Medica, Chinese Academy of Medical Sciences.

https://doi.org/10.1016/j.apsb.2021.08.016

**KEY WORDS**

Tea flower;
Exosome-like nanoparticle;
Breast cancer;
Metastasis;
ROS generation;
Microbiota modulation;
Intravenous injection;
Oral administration

**Abstract** Although several artificial nanotherapeutics have been approved for practical treatment of metastatic breast cancer, their inefficient therapeutic outcomes, serious adverse effects, and high cost of mass production remain crucial challenges. Herein, we developed an alternative strategy to specifically trigger apoptosis of breast tumors and inhibit their lung metastasis by using natural nanovehicles from tea flowers (TFENs). These nanovehicles had desirable particle sizes (131 nm), exosome-like morphology, and negative zeta potentials. Furthermore, TFENs were found to contain large amounts of polyphenols, flavonoids, functional proteins, and lipids. Cell experiments revealed that TFENs showed strong cytotoxicities against cancer cells due to the stimulation of reactive oxygen species (ROS) amplification. The increased intracellular ROS amounts could not only trigger mitochondrial damage, but also arrest cell cycle, resulting in the *in vitro* anti-proliferation, anti-migration, and anti-invasion activities against breast cancer cells. Further mice investigations demonstrated that TFENs after intravenous (i.v.) injection or oral administration could accumulate in breast tumors and lung metastatic sites, inhibit the growth and metastasis of breast cancer, and modulate gut microbiota. This study brings new insights to the green production of natural exosome-like nanoplatform for the inhibition of breast cancer and its lung metastasis *via* i.v. and oral routes.



## 1. Introduction

Breast cancer is the most commonly diagnosed cancer in females with high mortality, accounting for 11.6% of the total cancer-related death[1]. The major failure of breast cancer therapy is caused by high metastasis[2], and the lung is the most frequent metastatic site[3]. Nanotherapeutics (*e.g.*, Doxil®, Abraxane®, and NanoTherm®) are the promising options for practical treatment of breast cancer. However, the repeated administration of these standard nanotherapeutics results in undesirable therapeutic outcomes, serious adverse effects, and limited increase in overall survival rate[4,5]. Moreover, the high cost of large-scale production of these nanotherapeutics further impairs their clinical applications[6]. Therefore, it is urgent to exploit the next generation nanotherapeutics with the merits of good safety, high therapeutic effects, metastatic prevention, low cost, and easy scaled-up production, which would be beneficial for their medical translation to clinical treatment of breast cancers.

Exosomes are bilayer liposomal vesicles secreted by the living cells, which play critical roles in intercellular communication, signal transduction, and tumor metastasis[7–9]. Recently, mammalian cell-derived exosomes have been extensively employed in various biomedical fields, including drug delivery, disease diagnosis, and tissue reconstruction[10,11]. Although these exosomes are promising therapeutic nanoplatforms, their large-scale production and biohazard examination have been challenging[12]. Excitingly, plant cells also secrete exosome-like vesicles, which are biocompatible, cost-effective, eco-friendly, and mass-produced nanoplatforms[13]. Importantly, these platforms contain versatile bioactive compounds (*e.g.*, polyphenols, flavones, and functional proteins), and thus they have been applied in the treatment of various inflammatory and malignant diseases[14]. In recent ten years, numerous natural and green nanovesicles were facilely extracted from edible plants[15]. For instance, we extracted and purified ginger-derived nanoparticles (NPs) using a gradient centrifugation procedure. These NPs contained many active small molecules, which could greatly alleviate inflammation, improve intestinal repair, and prevent colitis and colitis-associated colorectal cancer *via* oral route. Importantly, these ginger-derived NPs caused no detectable adverse effects at the cellular and systemic levels[16]. Raimondo and colleagues produced natural NPs from lemon juice, and found that they could effectively inhibit the proliferation of cancer cells through the activation of TRAIL-mediated apoptotic cell death[17]. These NPs could also suppress the tumor growth *in vivo via* intraperitoneal administration and intratumor injection. Despite the short research history of edible plant-derived nanovesicles, they have already being tested in clinical trials for the treatment of colon cancer, head and neck cancer, and polycystic ovary syndrome (https://clinicaltrials.gov/; NCT01294072, NCT03493984, and NCT01668849).

Tea is the secondary most consumed beverage worldwide. The flavors and health-promoting properties of tea leaves mainly stem from their large amounts of beneficial compounds, including epigallocatechin-3-gallate (EGCG), bioactive proteins, and polysaccharides[18,19]. Compared to tea leaves, tea flowers contain the similar functional components. However, most tea flowers have been discarded in the farm, and their applications, especially in the medical field, have been seldom reported[20]. Since the benefits of plant-derived nanovesicles are largely dependent on their bioactive contents[21], it is rational to speculate that tea flower-derived nanovesicles are enriched in various bio-functional molecules and can be utilized as a novel therapeutic nanoplatform. In the present study, we for the first time to isolate exosome-like NPs from tea flowers (TFENs, Scheme 1A), and characterized their physicochemical properties (*e.g.*, contents, particle size, zeta potential, and morphology). Subsequently, their anti-breast cancer, anti-migration, anti-invasion, and pro-apoptotic activities and the corresponding underlying mechanisms were investigated. The accumulation profiles of TFENs in subcutaneous breast tumors and lung metastatic sites were studied, and their therapeutic potential against metastatic breast cancer was also evaluated *in vivo* (Scheme 1B). This study will shed light on the application of natural NPs in the treatment of parenteral cancers (metastatic breast cancer) *via* oral route.

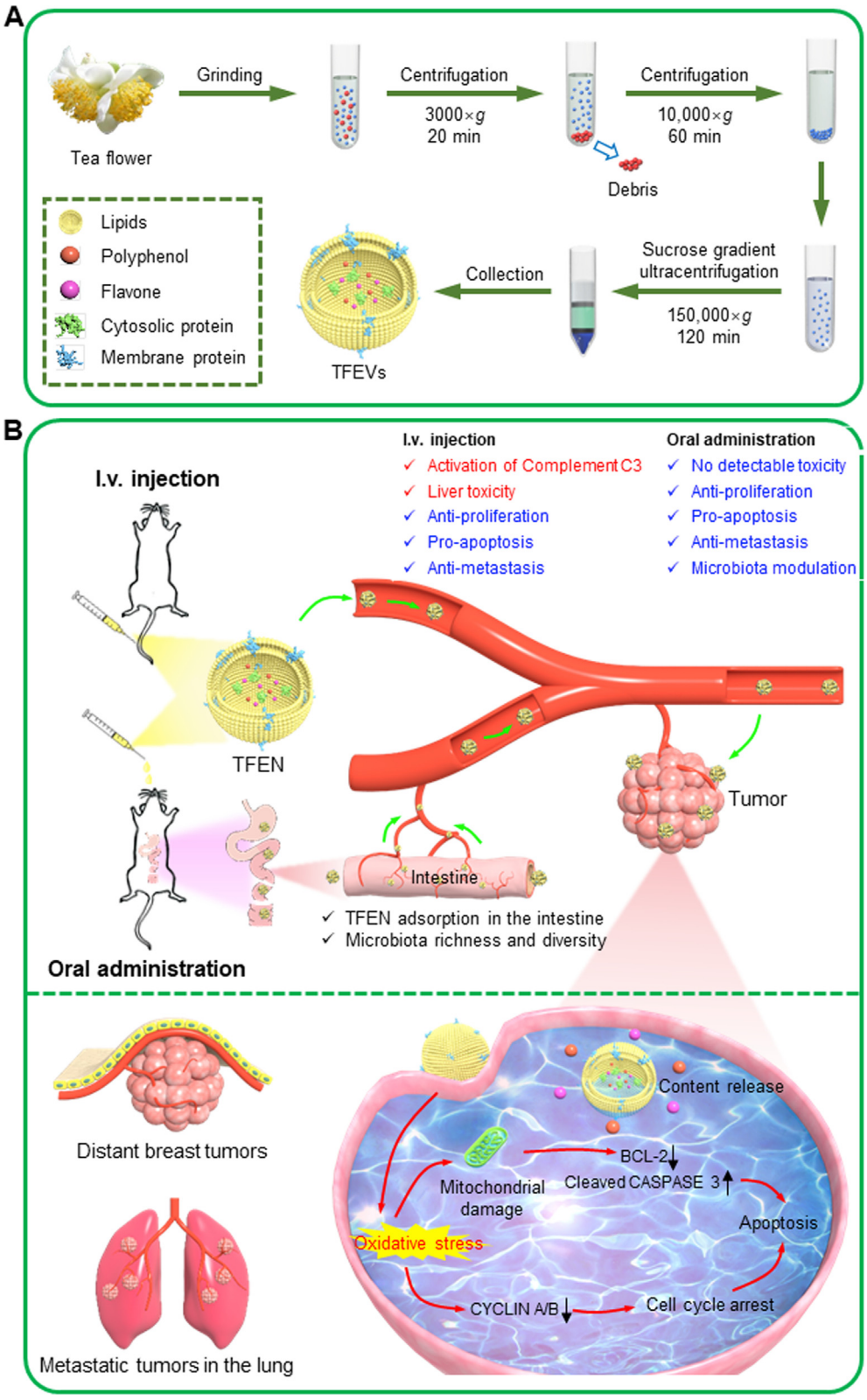


**Scheme 1** Schematic illustration of the production process of TFENs and their sequential treatment against metastatic breast cancers. (A) Schematic diagram of the extraction and purification of TFENs. (B) Scheme of the transportation and therapeutic functions of TFENs, including the transportation of TFENs after i.v. injection and oral administration, increased oxidative stress, mitochondrial damage, cell cycle arrest, and cell apoptosis.

## 2. Materials and methods

### 2.1. Materials

Fresh tea flowers (*Camellia sinensis* [L.] O. Kuntze) were obtained from Chongqing Ersheng Tea Co., Ltd. (Chongqing, China). Sucrose was purchased from Adamas-beta (Shanghai, China). Alexa Fluor 633 (AF633)-labeled phalloidin, 3,3′-dioctadecyloxacarbocyanine perchlorate (DiO), 1,1′-dioctadecyl-3,3,3′,3′-tetramethylindotricarbocyanine iodide (DiR), and a live/dead cell viability assay kit were from Thermo Fisher Scientific (Waltham, MA, USA). 4′,6-Diamidino-2-phenylindole (DAPI), 3-(4,5-dimethylthiazol-2-yl)-2,5-diphenyltetrazolium bromide (MTT), reactive oxygen species (ROS) assay kit, dichlorodihydro-fluorescein diacetate (DCFH-DA), dihydroethidium (DHE), 4-amino-5-methylamino-2′,7′-difluorofluorescein diacetate (DAF-FM DA), Hematoxylin & Eosin (H&E) Staining Kit, paraformaldehyde solution, Mitochondrial Membrane Potential Detection Kit, Cell Cycle Analysis Kit, and TdT-mediated dUTP Nick-End Labeling (TUNEL) Apoptosis Assay Kit were obtained from Beyotime Institute of Biotechnology (Shanghai, China). Annexin V-FITC Apoptosis Detection Kit was from 4 A Biotech Co., Ltd. (Beijing, China). BCA protein assay kit and Bouin's solution were purchased from Beijing Solarbio Science & Technology Co., Ltd. (Beijing, China). Novus Valukine™ ELISA kits (TNF-$\alpha$, IL-6, and IL-12) were purchased from R&D Systems (Minneapolis, MN, USA). Fetal bovine serum (FBS) was from Shanghai ExCell Bio, Inc. (Shanghai, China). Anti-cleaved CASPASE 3, anti- BCL -2, anti-CYCLIN A, anti-CYCLIN B, and anti-GAPDH antibodies were purchased from Novus Biologicals (Littleton, CO, USA). Alanine Aminotransferase Assay Kit, Alkaline Phosphatase Assay Kit, Aspartate Aminotransferase Assay Kit, Urea Assay Kit, Creatinine Assay Kit, And Complement three Assay Kit were from Nanjing Jiancheng Bioengineering Institute (Nanjing, Jiangsu, China). All other reagents and chemicals were of analytic grade and used as received.

### 2.2. Isolation and purification of TFENs

TFENs were isolated and purified following previous studies[16,22]. Tea flowers and phosphate-buffered saline (PBS) solution (1:2, g/mL) were placed in a blender and chopped at a high speed for 5 min. The obtained juices were centrifuged at 3000×*g* for 20 min (Hitachi, CP100NX, Tokyo, Japan) and 10,000×*g* for 1 h to remove the large plant tissues and cell debris. Subsequently, TFENs were collected by ultracentrifugation at 150,000×*g* for 2 h, and re-suspended in PBS. To further purify TFENs, their suspension was transferred to a discontinuous sucrose gradient (8%, 15%, 30%, 45%, and 60%, *w/v*), and ultracentrifuged at 150,000×*g* for 2 h. Finally, TFENs in the 15%/30% layer were harvested and washed 3 times. The amounts of TFENs were quantified on the basis of their protein amounts, which were determined using a BCA protein assay kit. The resultant TFENs were stored at −80 °C.

### 2.3. In vitro anti-cancer activity of TFENs

MTT assay was performed to investigate the *in vitro* anti-cancer activities of TFENs. MCF-7 cells, 4T1 cells, A549 cells, and HeLa cells were grown in 96-well plates at a final density of $5 \times 10^4$ cells per well and incubated overnight. Thereafter, the complete culture medium was exchanged to serum-free medium containing TFENs (protein concentration: 0.5−64 μg/mL) and co-incubated for 24, 48, and 72 h, respectively. Cells were thoroughly rinsed with PBS to eliminate the excess NPs and incubated with MTT (0.5 mg/mL). After incubation for 3 h, MTT-contained medium was discarded, and dimethyl sulfoxide was added to each well before spectrophotometric measurements at 570 nm. Cells without treatment were utilized as a negative control, whereas Triton X-100 (0.5%, *w/v*)-treated cells were used as a positive control.

### 2.4. Cell apoptosis assay

Annexin V-FITC/PI-staining assay was performed to quantify the pro-apoptotic activity of TFENs. Briefly, MCF-7 and 4T1 cells were seeded in 6-well plates at the same density of $5 \times 10^5$ per well and incubated overnight. Cells were exposed to TFEN suspensions (16 μg/mL, 2 mL) for 4 and 8 h, respectively. After being washed 3 times with PBS to eliminate the excess NPs, the cells were collected and stained using Annexin V-FITC Apoptosis Detection Kit. Finally, cells were analyzed immediately by flow cytometry (FCM, ACEA Novocyte™, 3130, San Diego, CA, USA) based on 10,000 gated cell events. Besides, proteins in cells were harvested in RIPA buffer to analyze the expression levels of apoptosis-related proteins (*cleaved* CASPASE *3* and BCL-2) by Western blot assay.

### 2.5. Changes of mitochondrial membrane potential

To visually evaluate the early apoptotic profiles of cells, the variations of mitochondrial membrane potentials were determined using a fluorescent probe (JC-1). In brief, MCF-7 cells and 4T1 cells were seeded in 24-well plates at a density of $1 \times 10^5$ per well and incubated overnight. Cells were exposed to TFEN suspensions (16 μg/mL, 1 mL) for 4 h. JC-1 solution and DAPI solution were applied to stain mitochondrial membrane and nucleus, respectively. Finally, fluorescent images were acquired immediately using a confocal laser scanning microscope (CLSM, Zeiss, LSM800, Jena, Germany).

### 2.6. Cell cycle assay

MCF-7 cells and 4T1 cells were seeded in 6-well plates at a density of $5 \times 10^5$ per well and incubated overnight. Cells were exposed to TFEN suspensions (16 μg/mL, 2 mL) for 24 and 48 h, respectively. Cells were collected, washed 3 times with PBS, and fixed in cold ethanol solution (70%, *v/v*) for 12 h. Thereafter, cells were treated by PI staining solution and RNase A solution for 30 min, and DNA contents were recorded using FCM (ACEA Novocyte™) based on 10,000 gated cell events. To further evaluate cell cycle inhibition profiles, the relative expression levels of cycle proteins (CYCLIN A and CYCLIN B) were determined using Western blotting analysis.

### 2.7. Generation of intracellular oxidative stress

MCF-7 cells and 4T1 cells were seeded in 24-well plates at a density of $1 \times 10^5$ per well and incubated overnight. Cells were exposed to TFEN suspensions (16 μg/mL, 1 mL) for 4 h. Subsequently, fluorescent probes (DCFH-DA, DHE, and DAF-FM DA) were added into each well. After staining for 30 min, cells were washed with PBS, and their nuclei were stained by DAPI for 20 min. Finally, the fluorescence intensities of cells were analyzed

by FCM (ACEA Novocyte™) based on 10,000 gated cell events, and the fluorescent images were acquired by a CLSM (Zeiss).

### 2.8. Cell migration assay

Scratch assay was conducted to evaluate the anti-migration capacities of TFENs against MCF-7 cells and 4T1 cells. Cells were seeded in 6-well plate at a density of $5 \times 10^5$ per well and culture for 48 h. The confluent cell monolayers were wounded with a sterile p10 pipet tip. Thereafter, cells were gently washed, and the wounds were imaged prior to/after the addition of TFEN suspensions (16 μg/mL, 2 mL) using an inverted fluorescence microscope (Leica microsystems, Bannockburn, IL, USA). The relative covering wound area was analyzed using Image J software (Wayne Rasband, Bethesda, MD, USA).

### 2.9. Transwell invasion assay

Cell invasion assay was carried out based on a Transwell plate (pore size: 8 μm; Nest Biotechnology, Wuxi, China)[23]. Briefly, MCF-7 cells and 4T1 cells were seeded into the upper chamber at a density of $5 \times 10^4$ per well and incubated overnight. The media in the upper chambers were replaced with serum-free media containing TFEN suspensions (16 μg/mL), and the media containing FBS (10%, *v/v*) were added into the lower chamber. FBS was used as a chemoattractant that attracted cells to cross membrane. Twenty-four hours after incubation, cells on the upper surface of membranes were scrubbed off with humid cotton buds, while cells on the bottom surface were immobilized with paraformaldehyde (1%, *v/v*) and stained with crystal violet (0.1%, *w/v*) for 30 min. Cells presented in the lower part of the inserts were determined by counting cells in 5 microscopic fields per well, and the migration profiles were expressed as an average number of cells per microscopic field.

### 2.10. In vivo inhibition of the growth and metastasis of breast cancer

BALB/c mice (6 weeks of age, female) and BALB/c nude mice (6 weeks of age, female) were purchased from Chengdu Dossy Biotechnology Company (Chengdu, Sichuan, China). All the animal cares and experiments were approved by Southwest University Institutional Animal Care and Use Committee. Human breast cancer MCF-7 xenograft tumor model was used to evaluate the *in vivo* anti-breast cancer capacity of TFENs. Briefly, MCF-7 cells ($5 \times 10^6$) were suspended in DMEM medium (100 μL) and subcutaneously injected in the right mammary gland of female BALB/c nude mice. When the average volumes of tumors reached 100 $mm^3$, mice were treated with TFENs (100 μL) at the concentrations of respective 1.5 or 3 mg protein/kg *via* intravenous (i.v.) injection or oral administration every other day. After 4 doses of TFEN treatment, mice were sacrificed by $CO_2$ inhalation. Tumors were collected, and their weights were measured. Tumors were fixed in paraformaldehyde solution (4%, *v/v*) for further pathological analysis, including H&E staining, TUNEL fluorescence staining, and Ki67 immunofluorescence staining.

Mouse lung metastasis model of breast cancer was established to evaluate the *in vivo* inhibition efficiency of TFENs against lung metastasis. Briefly, each female BALB/c mouse was injected with 4T1 cells at a density of $5 \times 10^4$ per mouse *via* tail vein injection. Two weeks after injection, mice were treated with TFENs *via* i.v. injection and oral administration. After 7 doses of TFEN treatment, mice were sacrificed by $CO_2$ inhalation. Lung tissues were collected and fixed in Bouin staining solution. The numbers of lung metastasis nodes were counted, and the nodes areas of lung tissues were examined by H&E staining.

## 3. Results

### 3.1. Physicochemical characterization of TFENs

TFENs were isolated and purified from fresh tea flowers using a differential centrifugation method coupled with sucrose density gradient ultracentrifugation (Fig. 1A). Transmission electron microscopy (TEM, Zeiss) was used to visualize the morphology of TFENs. It was obvious that these NPs were spherical exosome-like nanovesicles with a mean diameter of 20 nm (Fig. 1B). The dynamic light scattering (DLS, Malvern, Worcestershire, UK) examinations revealed that TFENs had an average hydrodynamic particle size of 131 nm with a relatively low polydispersity index (PDI, 0.155), as shown in Fig. 1C. The variations in average particle sizes of TFENs measured by TEM and DLS can be ascribed to the fact that TFENs were completely dehydrated for TEM test, whereas they are in a swollen state during DLS examination. Furthermore, the stabilities of TFENs were investigated in various simulating fluids. It was found that these NPs did not undergo any variations in particle sizes and zeta potentials in stomach simulating fluid, small intestine simulating fluid, and colon simulating fluid, as well as DMEM (Supporting Information Fig. S1), indicating that they could remain stable in the gastrointestinal tract (GIT) and blood after i.v. injection or oral administration.

The lipidomic results revealed that phosphatidylcholine (PC, ~26.6%), triglyceride (TG, ~23.4%), and phosphatidylethanolamine (PE, ~15.2%) were the major lipid compositions of TFENs (Fig. 1D and Supporting Information Table S1). Moreover, total proteins, including transmembrane proteins and intracellular proteins, were analyzed. The protein gel staining results implied that the molecular weight of all the proteins was over 15 kDa in TFENs (Fig. 1E). These protein components were further analyzed by proteomic analysis, and 745 kinds of proteins were found in TFENs by liquid chromatography coupled with tandem mass spectrometry (Fig. 1F). The Gene Ontology database and Genes and Genomes (KEGG) Annotation Path Analysis revealed that the proteins in TFENs were mainly related to cellular components, metabolism, and proliferation. In particular, 16 kinds of proteins were found to have oxidation-relevant functions (Supporting Information Table S2), indicating that these NPs might induce the increase of intracellular oxidative stress.

As reported, tea flowers contained lots of polyphenols and flavonoids, and these natural active molecules had the capacity to interfere with signaling pathways, gene expression processes, and cellular metabolisms, which involved apoptosis, migration, and immune responses[24–26]. Therefore, their contents in TFENs were quantified by high performance liquid chromatography–mass spectrometry. It was found that TFENs were enriched in several well-documented anticancer polyphenols and flavonoids, including EGCG, epicatechin gallate (ECG), epicatechin (EC), vitexin, myricetin-3-*O*-rhamnoside, kaempferol-3-*O*-galactoside, and myricetin (Fig. 1G and H). Collectively, TFENs can be considered as natural drug-loaded nanovesicles and have a promising potential in cancer treatment without loading additional drugs.

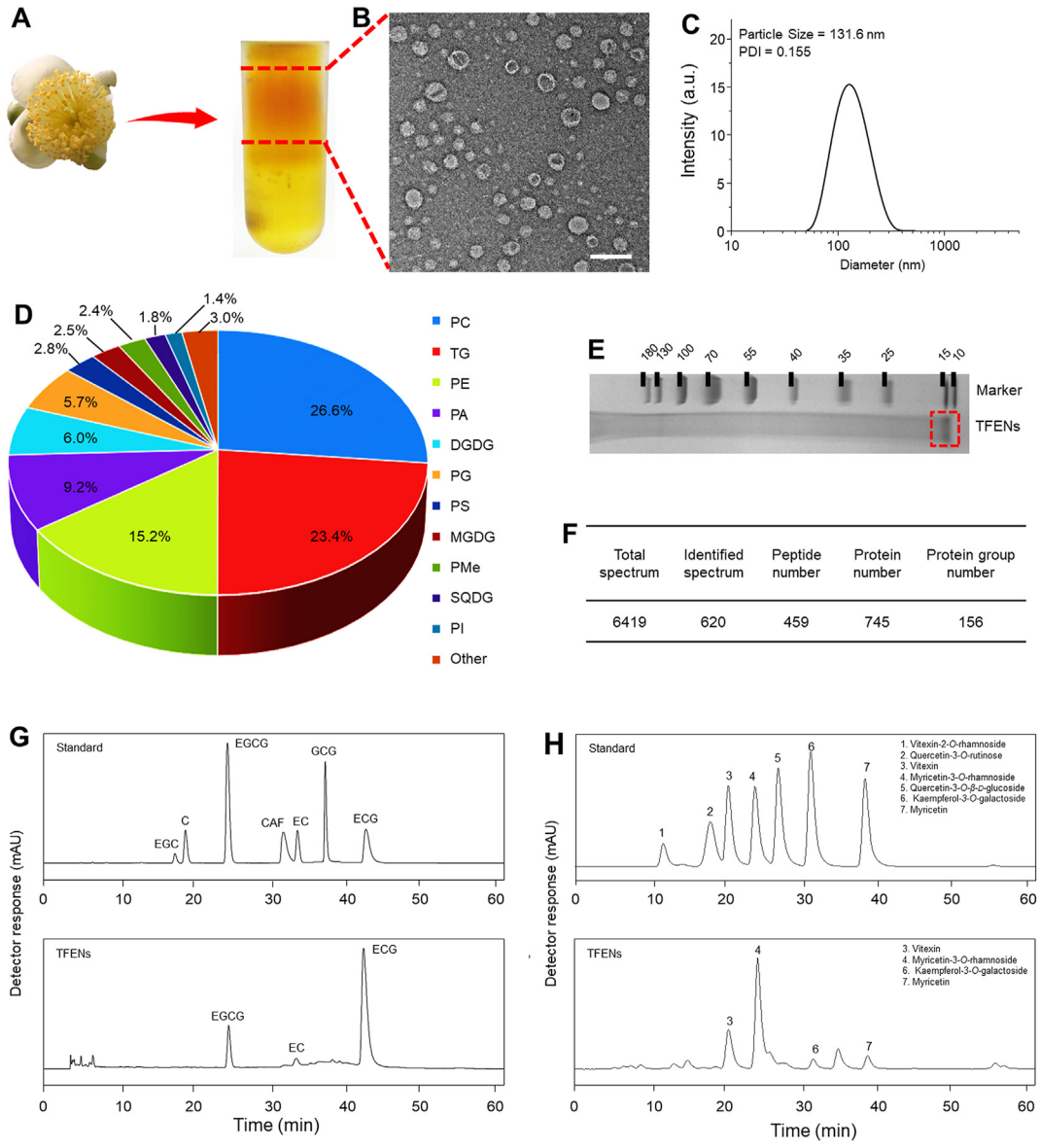


**Figure 1** Identification and physicochemical characterization of TFENs. (A) TFENs were isolated and purified by differential centrifugation and sucrose gradient ultracentrifugation. (B) TEM image (scale bar = 200 nm) and (C) hydrodynamic particle size of TFENs. The main components in TFENs (D) total lipids (E) proteins in SDS-PAGE gel (F) protein summary (G) polyphenols, and (H) flavonoids. PC, phosphatidylcholines; TG, triglyceride; PE, phosphatidylethanolamines; PA, phosphatidic acids; DGDG, digalactosyl diacylglycerols; PG, phosphatidylglycerol; PS, phosphatidylserine; MGDG, monogalactosyl diacylglycerols; PMe, phosphatidylmethanol; SQDG, sulphoquinovosyl diylyceride; PI, phosphatidylinositol; EGCG, epigallocatechin gallate; EC, epicatechin; ECG, epicatechin gallate.

### 3.2. *Uptake profiles of TFENs by cancer cells and GIT tissues*

The active contents of the natural NPs exert their biological functions mainly within cells, and thus it is essential for their cellular uptake by cancer cells. A green fluorescence probe (DiO) was applied to label TFENs and track their biodistribution. The TFENs without loading of DiO had a hydrodynamic diameter of 118.1 nm, which was smaller than DiO-labeled TFENs (Supporting Information Fig. S2A and S2B). It was found that these two types of NPs showed comparable surface charge (around −7.6 mV, Fig. S2C). The cellular uptake percentages of DiO-labeled TFENs by MCF-7 cells (Fig. 2A) and 4T1 cells (Fig. 2B) were increased as incubation time extended. After co-incubation for 5 h, the cell internalization percentages of DiO-labeled TFENs by MCF-7 cells and 4T1 cells were 94.4% and 49.9%, respectively, indicating that TFENs were more preferentially internalized by these cells. The mean fluorescence intensity (MFI) values (Fig. 2A and B) were in good agreement with these results. Previous studies implied that the phagocytic efficiencies of NPs depended on the receptors on the surface of cells[27,28]. Therefore, the differences in the internalization efficiencies of TFENs might be due to the heterogeneous surface contents between MCF-7 cells and 4T1 cells. Fig. 2C showed that DiO-labeled TFENs (green fluorescence) were obviously internalized by MCF-7 cells and 4T1 cells, and these NPs mainly distributed around the nucleus (Fig. 2D).

Oral route has been considered the most convenient approach for drug administration, as it has the merits of ease of daily administration, patient compliance, and wide therapeutic

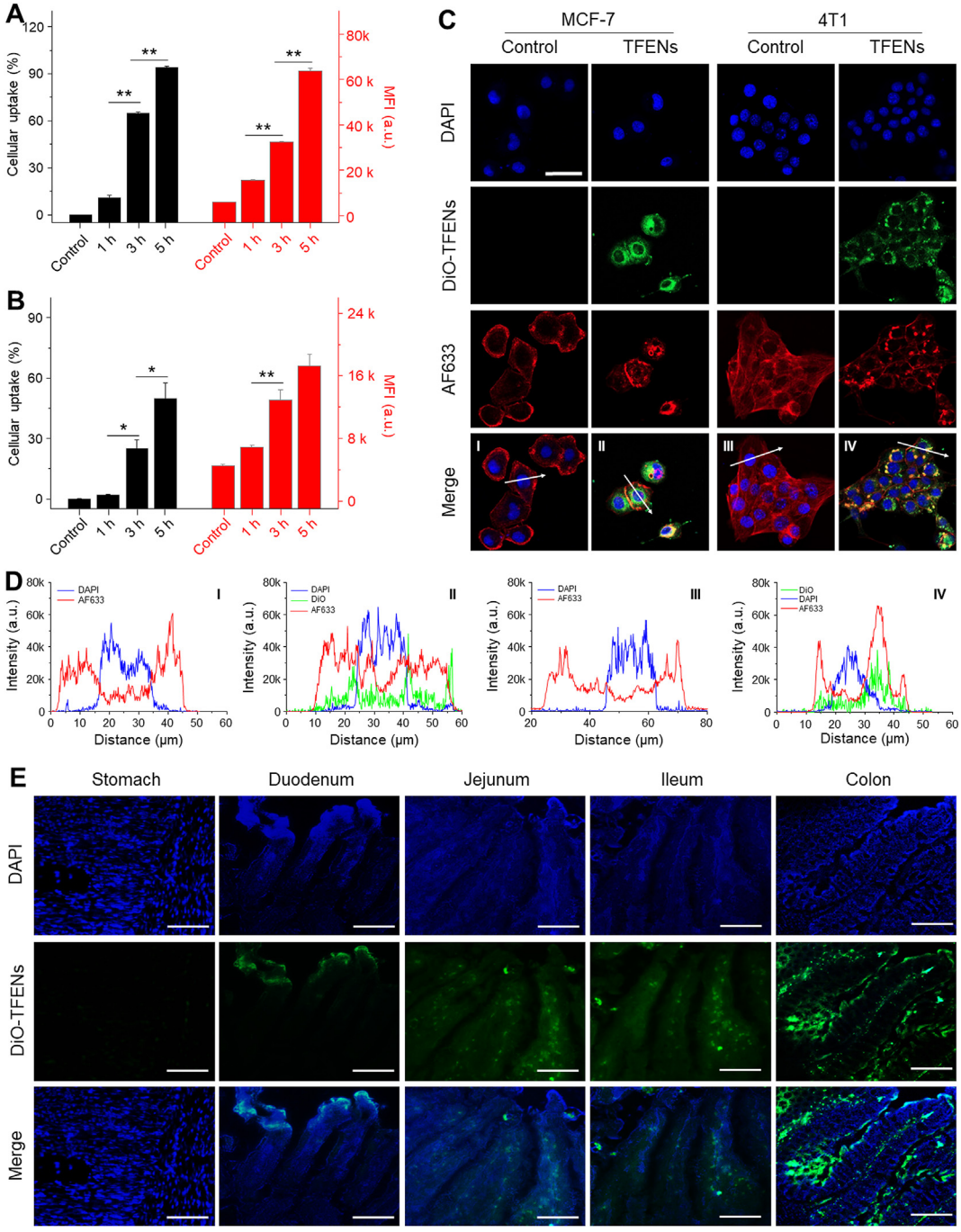


**Figure 2** Uptake profiles of TFENs by cancer cells and intestinal tissues. FCM analysis of the cellular uptake profiles of DiO-labeled TFENs in (A) MCF-7 cells and (B) 4T1 cells for 1, 3, and 5 h, respectively. Each point represents the mean ± SEM ($n = 3$). *$P < 0.05$, **$P < 0.01$. ns, no significance. (C) Confocal microscopy images and (D) fluorescence distribution profiles of MCF-7 and 4T1 cells receiving the treatment of DiO-labeled TFENs (scale bar = 20 μm). (E) Distribution of TFENs in different sections of GIT (stomach, duodenum, jejunum, ileum, and colon) from the mice with the treatment of DiO-labeled TFENs at the time point of 6 h (scale bar = 50 μm).

window[23,29]. To determine the adsorption sites of oral TFENs from the GIT to the circulatory system, their distribution in the GIT was investigated. Mucus is a protective layer of intestinal epithelium, which has been recognized as an important physiological barrier for oral NPs[30]. Supporting Information Fig. S3A reveals that TFENs could freely diffusion in the simulating mucus. Mean-square-displacement (MSD) values reflect the locomotive behaviors of NPs in biological fluids[31]. TFENs had a strong moving capacity in the simulating mucus (Fig. S3B). Further *in vivo* experiments indicated that after oral administration of DiO-labeled TFENs (5 mg/kg), NPs (green) were observed in the mucosas of the jejunum, ileum and colon, implying that TFENs could efficiently penetrate through the intestinal epithelial layer and be absorbed into blood (Fig. 2E).

### 3.3. *In vitro anti-proliferation, pro-apoptotic, and anti-mobility activities of TFENs*

Considering that TFENs contained an impressive amount of anti-cancer molecules, their anti-cancer activities were evaluated by MTT assay. These NPs showed obvious anti-cancer capacities against MCF-7 cells, 4T1 cells, A549 cells, and HeLa cells after co-incubation for different time periods (24, 48, and 72 h), and these anti-cancer profiles presented both dose-dependent and time-dependent manners (Fig. 3A). At the meantime, we found that at a low protein concentration (0.5 μg/mL), TFENs exerted promotion effect on MCF-7 cells. This result can be attributed to the fact that these natural NPs at low doses might be treated as nutrient substances. Conversely, they would show anti-cancer activities at higher protein concentrations. Notably, very weak cytotoxicities were found in the normal cell lines (HUVEC cells and HEK293T cells) after the treatment of TFENs, revealing their good biocompatibility. Furthermore, the half maximal inhibitory concentrations ($IC_{50}$) of TFENs in different cell lines were calculated and showed in Fig. 3B. We found that TFENs exhibited relatively stronger anti-proliferation capacities against breast cancer cell lines (MCF-7 cells and 4T1 cells) than A549 cells and HeLa cells. In addition, at the time point of 72 h, the $IC_{50}$ values of TFENs against HUVEC cells and HEK293T cells were tens to hundreds of higher than those against MCF-7 cells and 4T1 cells. The live/dead staining results revealed that clear red fluorescence signals were found in all the TFEN-treated cancer cell lines when compared with their

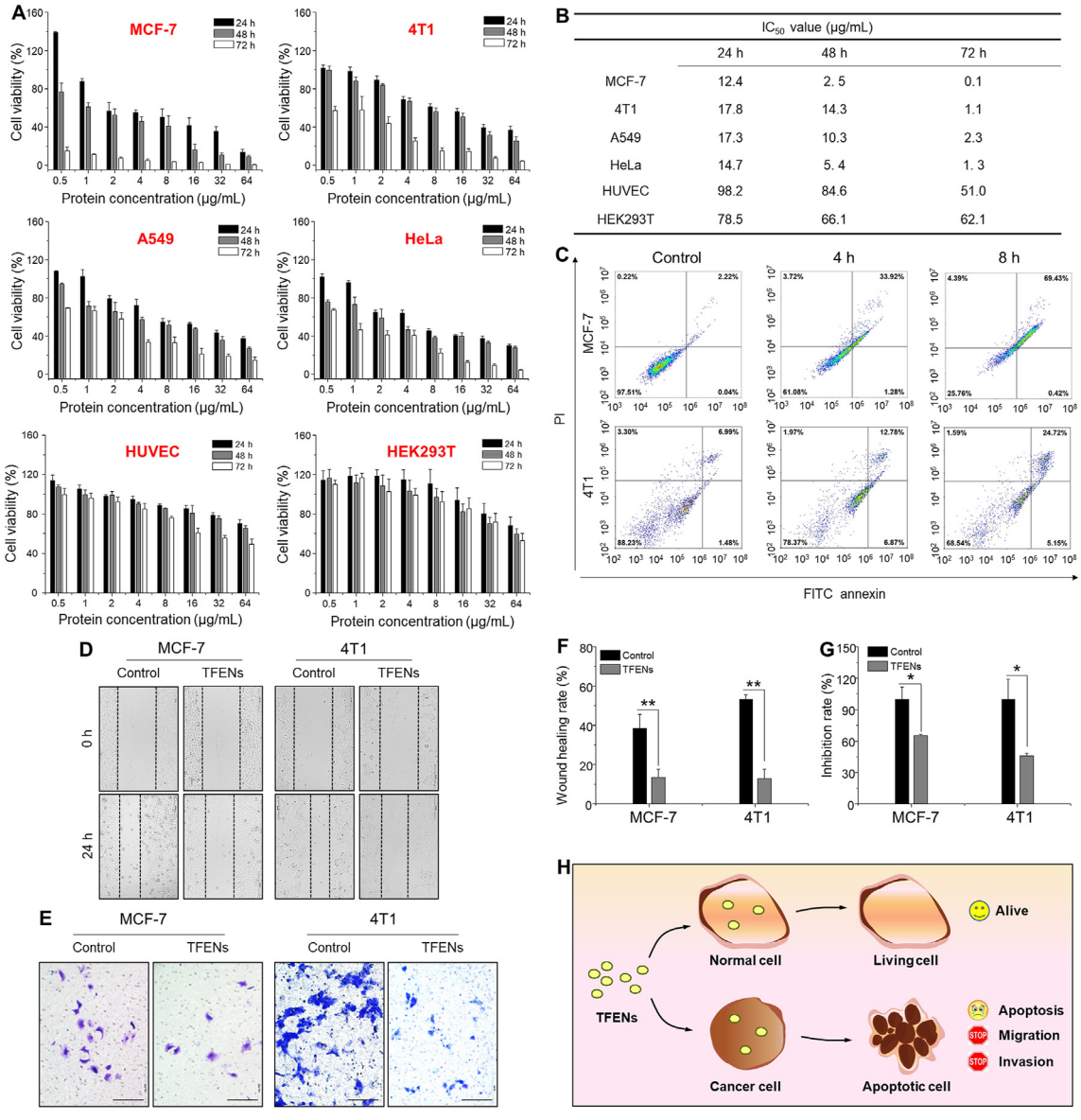


**Figure 3** *In vitro* anti-proliferation, pro-apoptotic, and anti-mobility properties of TFENs. (A) Viabilities of various cell lines with the treatment of TFENs for 24, 48, and 72 h, respectively, and (B) their corresponding $IC_{50}$ values. Each point represents the mean ± SEM ($n = 5$). (C) Pro-apoptotic capacities of TFENs against MCF-7 cells and 4T1 cells after co-incubation for 4 and 8 h, respectively. (D, F) Migration and (E, G) invasion of MCF-7 cells and 4T1 cells with or without the treatment of TFENs for 24 h, and their corresponding quantitative results. Scale bar = 100 μm. Each point represents the mean ± SEM ($n = 3$). *$P < 0.05$, **$P < 0.01$. ns, no significance. (H) The schematic illustration of the impacts of TFENs on healthy cells and cancer cells.

corresponding control groups (Supporting Information Fig. S4), confirming the excellent broad-spectrum anti-tumor activities of TFENs. The different anti-proliferation activities of TFENs against various cancer cells might be mainly due to the different cellular uptake efficiencies.

Tea flower contents, including EGCG, EC, and ECG, were reported to exhibit anti-breast cancer activities by inducing apoptosis[32,33]. To verify the pro-apoptotic potentials of TFENs against breast cancer, an apoptosis assay was conducted, as shown in Fig. 3C. Very few cells were in apoptosis status in the control groups of MCF-7 and 4T1 cells. In the contrary, after incubation with TFENs for various time periods (4 and 8 h), significant proportions of apoptotic cells were found in both MCF-7 cells and 4T1 cells. We also found that higher percentages of apoptosis cells were found in the cell groups after 8 h of incubation (69.9% of MCF-7 cells and 29.9% of 4T1 cells) than those after 4 h of incubation (35.2% of MCF-7 cells and 19.7% of 4T1 cells), reflecting the time-dependent pro-apoptotic effect of TFENs (early apoptosis plus late apoptosis).

Tumor metastasis, one of the main factors inducing high mortality, is closely correlated with a fundamental cellular behavior called cell motility[34]. Thus, the cell motility inhibition abilities of TFENs were investigated by cell scratches and Transwell migration experiments. Fig. 3C and D indicates that the migrated and invaded cells in the control groups were extensively observed, indicating the intrinsic metastatic activity of breast cancer cells. However, TFEN treatments significantly decreased the wound closure rates of MCF-7 cells and 4T1 cells, and much less TFEN-treated cells migrated through the chamber, in comparison with the control cells. Moreover, the quantitative results in Fig. 3F and G confirm the anti-migration and anti-invasion properties of TFENs, demonstrating that these NPs had a strong capacity to inhibit the metastasis of breast cancer. The overall impacts of TFENs on healthy cells and cancer cells were schematically illustrated in Fig. 3H.

### 3.4. *Anti-cancer mechanism of TFENs*

As mentioned above, 16 kinds of proteins in TFENs were related to the intracellular oxidation (Table S2). Meanwhile, polyphenols and flavonoids were reported to induce the increase of oxidative stress in cancer cells[35,36]. Therefore, the intracellular oxidative elements of TFEN-treated cells were evaluated. The levels of intracellular ROS and superoxide anion (SA) were tracked by using DCFH-DA and DHE, respectively. As presented in Fig. 4A, significant increases in total ROS and SA were found in both MCF-7 cells and 4T1 cells after the treatment with TFENs. The quantitative results revealed that the total concentrations of ROS in the TFEN-treated MCF-7 cells and 4T1 cells were 14.2- and 9.3-fold higher than those in the corresponding control cells (Supporting Information Fig. S5). The SA amounts were elevated 73.8% in MCF-7 cells and 29.1% in 4T1 cells compared with the control cells (Supporting Information Fig. S6). Nitrogen monoxide (NO), one of the most common reactive nitrogen species (RNS), was visualized by a green fluorescence probe DAF-FM DA in both MCF-7 cells and 4T1 cells. It was found that the NO amounts were increased in these cells receiving the treatment of TFENs. Further quantitative investigations revealed that after co-incubation with TFENs for 4 h, the NO amounts showed 5.2- and 3.5-fold increases in MCF-7 cells and 4T1 cells, respectively (Supporting Information Fig. S7). These findings reveal that TFEN treatment is liable to stimulate the generation of oxidative stress in breast cancer cells. Moreover, the larger amounts of ROS, SA, and NO were found in TFEN-treated MCF-7 cells than those in TFEN-treated 4T1 cells, which might be a crucial contributing factor for the lower $IC_{50}$ value of TFENs against MCF-7 cells compared with those against 4T1 cells (Fig. 3B).

Since oxidative stress could trigger mitochondrial damage and cell cycle arrest[37], we assessed the impacts of TFENs on these two aspects. JC-1, as a mitochondrial membrane potential fluorescence probe, can be used to visualize the apoptotic cells. After the incubation with JC-1 probes, the negative control MCF-7 cells and 4T1 cells showed strong yellow fluorescence intensity (J-aggregates) due to the high mitochondrial membrane potential in the living cells (Fig. 4B). However, relatively weak green fluorescence signals (J-monomers) were detected in the TFEN-treated cells (MCF-7 and 4T1 cells), revealing that TFEN treatment could result in the mitochondrial damages. Mitochondria are known to play a central role in triggering the cappase signaling pathway-dependent apoptosis[38]. CASPASE-3 was a typical hallmark in apoptosis, and BCL-2 was an apoptotic inhibitory protein[39]. Here, we studied the variations of the expression levels of caspase-*3* and BCL-2 in MCF-7 cells and 4T1 cells after the treatment of TFENs for 24 and 48 h, respectively. As shown in Fig. 4C, the expression levels of activated caspase-*3* were obviously elevated in both MCF-7 cells and 4T1 cells receiving TFEN treatments. On the contrary, TFEN-treated cells showed much lower expression levels of BCL-2 than the control cells. These observations indicate that the pro-apoptosis of TFENs is based on the caspase-dependent pathways.

Subsequently, the cell cycle profiles of MCF-7 cells and 4T1 cells were investigated upon the treatment of TFENs. It was found that TFEN treatment induced different patterns of cell cycle arrests in MCF-7 (Fig. 4D) and 4T1 cells (Fig. 4E). The fraction of TFEN-treated MCF-7 cells in G0/G1 phase and S phase were remarkably reduced, in comparison with the control MCF-7 cells. Furthermore, more MCF-7 cells were found in G2/M phase as the elongation of incubation time, implying that TFENs could efficiently inhibit the mitosis process of MCF-7 cells. In the context of 4T1 cells, the treatment of TFENs induced cell cycle arrest at S phase, demonstrating that TFENs were capable to block DNA replication in 4T1 cells. Many cycle proteins are critical for the progress of cell cycle, and thus the expression profiles of two typical cell cycle-regulating proteins (cyclin A and cyclin B) were evaluated. Fig. 4F shows that after the treatment of TFENs for 24 and 48 h, MCF-7 cells and 4T1 cells presented time-dependent decreases in the expression levels of cyclin A and cyclin B compared with the corresponding control cells, leading to the cell cycle arrest and the subsequent cell apoptosis. The schematic illustration of pro-apoptotic processes of TFENs is presented in Fig. 4G. In addition, we measured the intracellular oxidative elements (ROS, SA, and NO) and mitochondria damage induced by TFENs in HUVEC cells. It was found that HUVEC cells showed few oxidative elements in their cytoplasms and slight mitochondrial damage after the treatment of TFENs (Supporting Information Fig. S8). Therefore, we can conclude that the selective cytotoxicities of TFENs against tumor cells stem from the induction of high oxidative pressure in these cells, not in the healthy cells (*e.g.*, HUVEC cells).

### 3.5. *In vivo anti-breast cancer effect of TFENs*

Both i.v. injection and oral administration are common drug administration approaches. To investigate the *in vivo* distribution

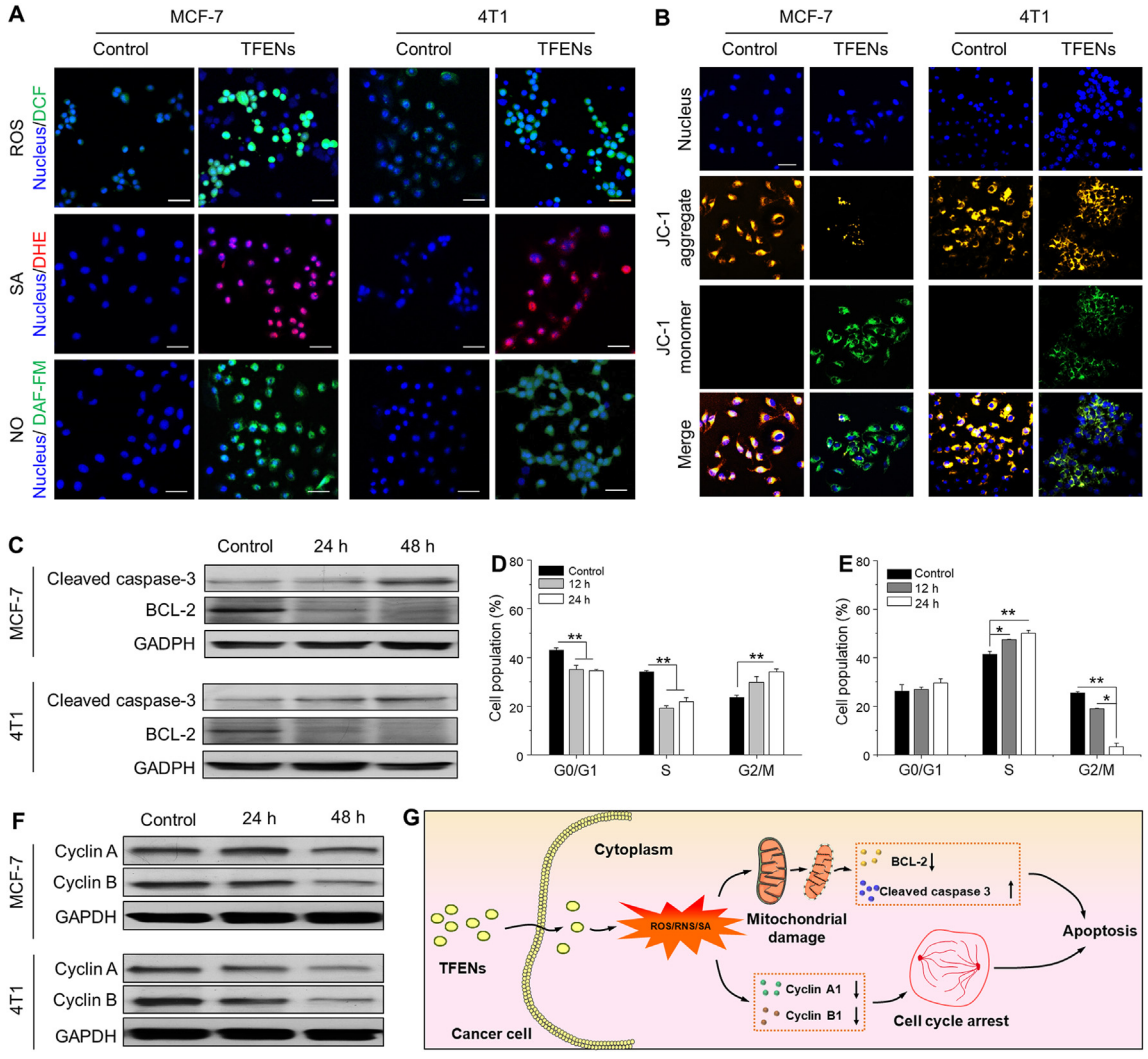


**Figure 4** Confocal microscopy images of (A) ROS, SA, NO, and (B) mitochondrial membrane potential changes in MCF-7 cells and 4T1 cells after the treatment of TFENs for 4 h (scare bar: 50 μm). (C) Western blot analysis of cleaved caspase-3 and BCL-2 in MCF-7 cells and 4T1 cells receiving the treatment of TFENs for 24 and 48 h, respectively. Cell population profiles of (D) MCF-7 and (E) 4T1 cells in various cell cycle phases after co-incubation for 12 and 24 h, respectively. Each point represents the mean ± SEM ($n = 3$). *$P < 0.05$, **$P < 0.01$. ns, no significance). (F) Western blot analysis of cyclin A and cyclin B in MCF-7 cells and 4T1 cells receiving the treatment of TFENs for 24 and 48 h, respectively. (G) Schematic illustration of the pro-apoptotic mechanism of TFENs against cancer cells.

of TFENs, DiR molecules were encapsulated into TFENs. As seen in Fig. 5A, TFENs were gradually accumulated in the tumor tissues for both administration routes. The maximum accumulating amount of TFENs in the tumor tissues was found at the time point of 24 h after i.v. injection. However, this phenomenon was observed at 48 h post oral administration. Moreover, the maximum MFI of the tumor tissues in the TFEN (i.v.)-treated group was much stronger than that in the TFEN (oral)-treated group. Next, the distribution profiles of TFENs in the five major organs (heart, liver, spleen, lung, and kidney) were investigated. Large amounts of TFENs after i.v. injection and oral administration were detected in the liver and lung, and their fluorescence signals in these two organs decayed rapidly after 24 h of administration. Notingly, the second most preferentially accumulating site of TFENs was lung, which was one of the most common metastatic sites for metastatic breast cancer. Therefore, it was speculated that TFENs might have the potential to inhibit lung metastasis of breast cancer. To verify the beneficial role of TFENs in oral delivery of their components, the *in vivo* distribution profile of free DiR molecules was also determined. It was found that very few fluorescence dye (DiR) was distributed in the five main organs after oral administration (Supporting Information Fig. S9), in comparison with the mouse group receiving oral DiR-loaded TFENs. These observations imply that oral TFENs can maintain stable in GIT, facilitate the loaded contents to transport through the intestinal barriers, enter the circulatory system, and accumulate in the tumor sites.

To evaluate the therapeutic effects of TFENs against breast cancer, a subcutaneous xenograft breast tumor model was established, which was treated with TFENs once every 2 days at a dose of 1.5 (low) or 3.0 (high) mg/kg *via* i.v. injection and oral administration, respectively. Mouse body weights and tumor sizes were recorded every day after the average tumor sizes reached 100 $mm^3$. Fig. 5B shows that an obvious body weight loss was found in the TFEN-treated group (i.v., high), which was dramatically declined to 81.4% on Day 9 when compared with that on Day 0. However, the body weights of the other mouse groups

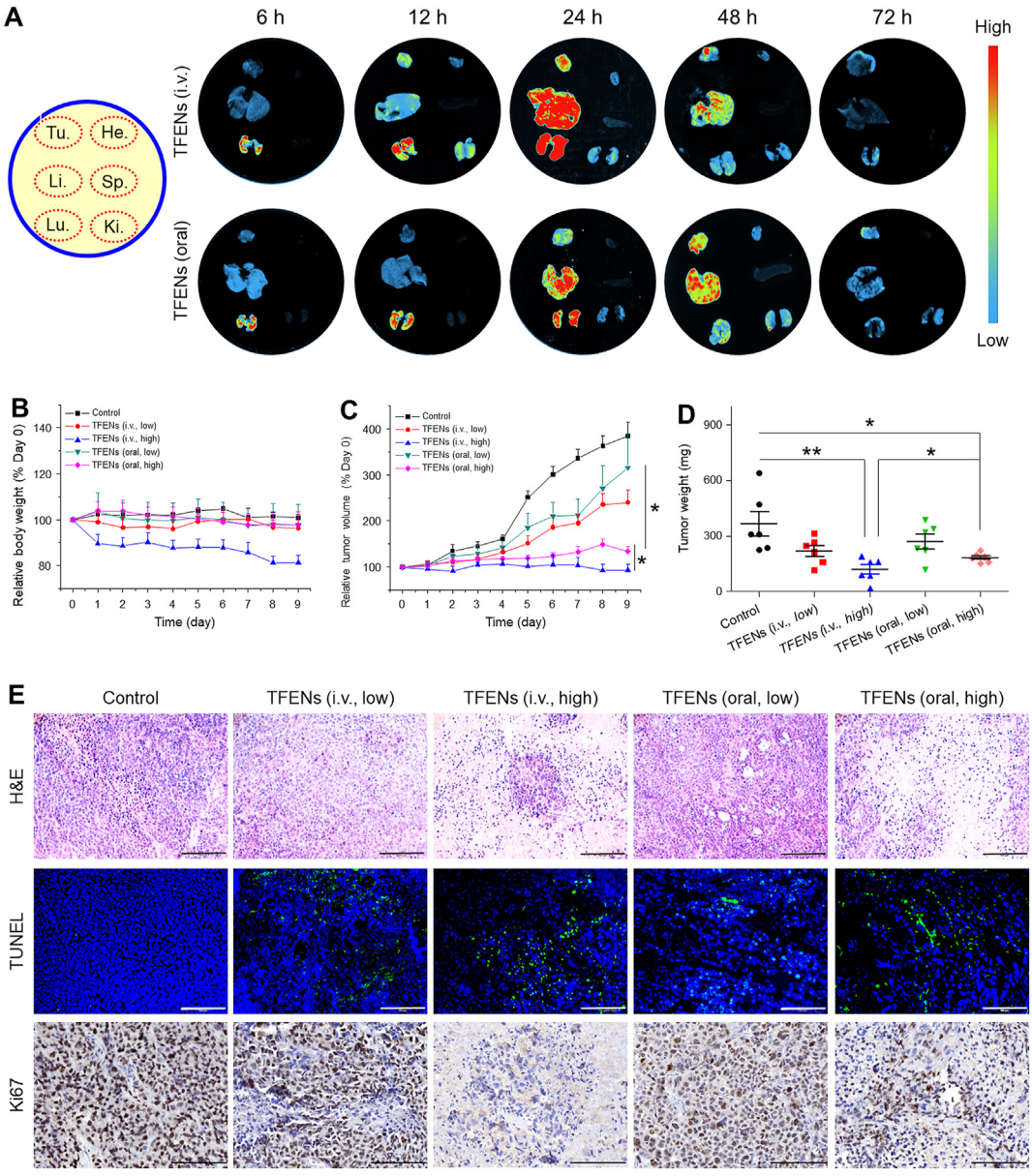


**Figure 5** *In vivo* bio-distribution and anti-cancer activities of TFENs based on a subcutaneous xenograft breast tumor model. (A) *In vivo* bio-distribution of DiR-loaded TFENs in tumor, heart, liver, spleen, lung, and kidney at different time points (6, 12, 24, 48, and 72 h). (B) Relative body weight variations and (C) tumor volume variations over 9 days after the treatment of TFENs *via* i.v. injection and oral route. (D) Tumor weights on day 9. (E) Histological analysis of resected tumor sections from different treatment groups through H&E staining, TUNEL assay, and Ki-67 staining (scale bar = 100 μm). Each point represents the mean ± SEM ($n = 6$). *$P < 0.05$, **$P < 0.01$. ns, no significance.

maintained stable during the entire investigation. These observations indicate that TFEN treatment at a high dosage might cause serious toxicities.

As observed in Fig. 5C and Supporting Information Fig. S10, the tumor sizes of the control group progressed rapidly over 9 days, whereas the growth trend of tumors was remarkably retarded by TFENs. It was worth noting that TFEN treatment (i.v., high) fully inhibited tumor growth (Supporting Information Fig. S11). Although the TFEN-treated group (oral, high) showed less tumor inhibition ratio than the TFEN-treated group (i.v., high), no significant statistical significance was detected between these two mouse groups. In addition, the average tumor weight of the TFEN-treated group (i.v., high) was 117.6 mg, which was much lighter than that of the other treatment groups (Fig. 5D). To explore the *in vivo* antitumor mechanism of TFENs, tumor tissues from various mouse groups were sectioned and stained by H&E, TUNEL, and Ki67.

As seen in Fig. 5E, H&E staining images reveal that high-density of cancer cells were observed in the tumor tissues from the control group, and necrotic cancer cells were hardly detected. In contrast, all the TFEN-treated groups showed much less tumor cell numbers compared with the control group, and clear pyknosis and apoptotic bodies were observed in these groups. Subsequently, a TUNEL assay was performed to verify the apoptotic profiles of the tumor tissues from various groups. The control group presented no evident apoptosis in its tumor tissues, whereas the percentages of apoptotic cells were significantly elevated in all the TFEN-treated groups. In particularly, the highest percentage of

apoptotic cells was found in the TFEN-treated group (i.v., high), and the TFEN-treated group (oral, high) also showed relatively high percentage of apoptotic cells (Supporting Information Fig. S12), suggesting that TFENs with high dosages could effectively trigger tumor apoptosis *in vivo* regardless of i.v. injection and oral administration. Additionally, the *in vivo* anti-proliferation activities of TFENs were assessed by Ki67 staining (Supporting Information Fig. S13). The numbers of Ki67-positive tumor cells were in negative correlation with the TUNEL staining results, confirming the strong tumor inhibition capacities of TFENs at high dosages.

### 3.6. *In vivo inhibition effect of TFENs on lung metastasis*

Breast tumors preferentially metastasize to the lungs, which have been known as a main cause for mortality[40]. To assess the inhibitory effect of TFENs on lung metastasis, a lung metastasis mice model was established. Initially, the *in vivo* biodistribution profiles of TFENs were evaluated. Fig. 6A reveals that the strongest signals and the longest retention time were found in the lungs with metastatic breast cancers for both administration approaches (i.v. injection and oral route). Furthermore, the maximum accumulating amounts of TFENs in the lungs for i.v. injection and oral administration were reached at the time points of 12 and 24 h, respectively. In addition, more TFENs were accumulated in the lungs from the TFEN-treated group (i.v., high) than those from the TFEN-treated group (oral, high). The specific accumulation of TFENs in lung metastases provides an essential prerequisite for the treatment of metastatic breast cancer. The diverse distribution profiles of TFENs presented in Figs. 5A and 6A were attributed to the different mouse models (subcutaneous tumors and metastatic breast tumors) used in these two animal experiments.

To investigate the anti-lung metastasis effect of TFENs, after i.v. injection of 4T1 cells, mice with lung metastatic sites were treated with TFENs. Although no statistical significance was found in the body weight losses among all the mouse groups, the TFEN-treated group (i.v., high) presented the lowest body weight (Fig. 6B). As expected, the numbers of tumor nodes within the lung tissues were substantially decreased in all the TFEN-treated groups (Fig. 6C and Supporting Information Fig. S14). Furthermore, the strongest anti-lung metastasis effect was obtained by the i.v. injection of TFENs at a high dose (91.4% inhibition rate), as shown in Fig. 6D. Surprisingly, there was no statistical difference between the TFEN-treated group (i.v., high) and the TFEN-treated group (oral, high), indicating that the administration of TFENs *via* oral route could achieve the comparable therapeutic effect as i.v. injection did. The H&E staining of lung tissues was performed to confirm the therapeutic effect of TFENs. As shown in Fig. 6E, abundant metastatic lesions were observed in the control group, whereas only sporadic lesions could be found within lung tissues from the TFEN-treated group (i.v., high) and the TFEN-treated group (oral, high).

Gastrointestinal microbiota plays an important role in regulating the homeostasis of bodies through the generation of

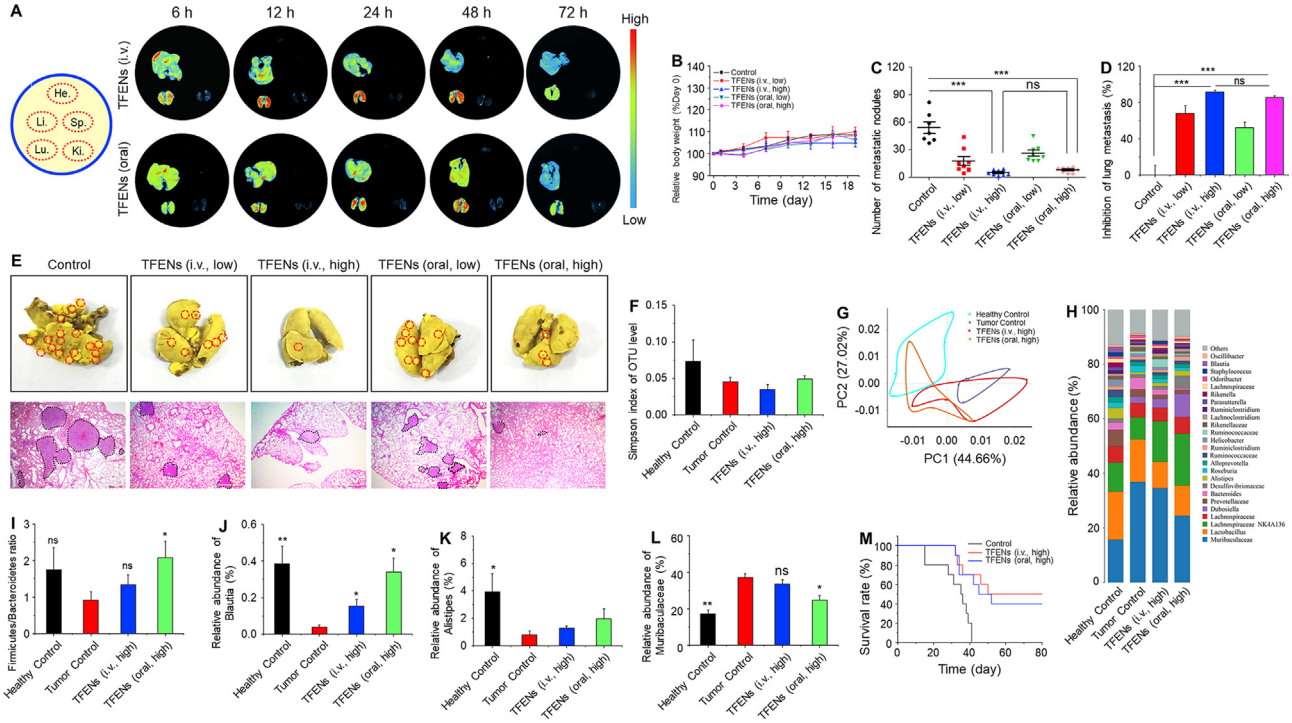


**Figure 6** *In vivo* bio-distribution and anti-metastasis activities of TFENs based on lung metastasis model of breast cancer. (A) *In vivo* bio-distribution of DiR-loaded TFENs in heart, liver, spleen, lung, and kidney at different time points (6, 12, 24, 48, and 72 h). (B) Relative body weight variations over 9 days after the treatment of TFENs *via* i.v. injection and oral route. (C) Total numbers of metastatic tumor nodules and (D) lung metastasis inhibition profiles of TFENs at the end of experiments. (E) Representative images and H&E staining of the lungs from different treatment groups on day 19 (scale bar = 100 mm). Microbiome analysis of the fecal samples. (f) $\alpha$-Diversities were presented by box plot of the Simpson indexes. (G) Principle component analysis (PCA) plots of gut microbiota. (H) Gut microbiota compositions in different treatment groups at the genus level. (I–L) Relative abundances of the typical beneficial bacteria and harmful bacteria in different treatment groups. (M) Survival rates for each group receiving different treatments. Each point represents the mean ± SEM ($n = 8$). *$P < 0.05$, **$P < 0.01$. ns, no significance.

metabolites, hormones, and inflammatory factors[41−43]. It has been demonstrated to influence the therapeutic outcomes of drug formulations against host diseases[44,45]. Very recently, Rosean and coworkers[46] firstly reported that dysbiosis of gastrointestinal microbiota promoted the metastasis of breast tumors in a murine model. Another report revealed that the treatment of antibiotics would disrupt the microbiota balance, resulting in the increased metastasis risk of breast tumor[47]. However, few attempts have been made to investigate the relationships among nanotherapeutics, intestinal microbiota, and metastatic breast cancer. Therefore, we comparatively analyzed the microbial compositions of feces from different treatment groups. It was found that the healthy control group showed the highest Simpson index of the operational taxonomic unit (OTU) level among all the groups. Moreover, the Simpson index of the OTU level in the TFEN-treated group (oral, high) was higher than those in the tumor control group and the TFEN-treated group (i.v., high, Fig. 6F), suggesting that TFEN treatment *via* oral route could greatly increase the community abundance and diversity of gastrointestinal microbiota. The imbalance of microbial environment was reported to exacerbate immune responses and decrease the production of anti-proliferative metabolites, which could induce the migration of tumor cells into the lymph nodes or circulatory system, and to the lungs[48]. The beneficial effects of oral TFENs on the abundance and diversity of microbiota were consistent with their anti-metastatic capacity of breast cancer.

Next, the cylindrical coordinate analysis (PCoA) was performed to evaluate the microbiota similarities among these mouse groups, and the distances between each two groups exhibited the certain variations in PCoA axes. We found that the distances between the healthy control group and the TFEN-treated group (oral, high) were much shorter compared with that between the healthy control group and the tumor control group/the TFEN-treated group (i.v., high, Fig. 6G), reflecting that oral administration of TFENs could maintain the stability of intestinal microbiota. The relative abundance of gut microbiota presented the overall variations among these four mouse groups at the genus level (Fig. 6H). The Firmicutes/Bacteroidetes (F/B) ratio in the healthy control group was higher than that in the tumor control group, which was comparable to that in the TFEN-treated group (oral, high). Furthermore, TFEN treatment *via* oral route could maintain the abundance of the typical beneficial symbiotic bacteria (Fig. 6I–K) and decrease the abundance of the typical harmful bacteria (Fig. 6I). Finally, the survival rates of different mouse groups with lung metastasis were assessed. It was found that TFEN treatment could obviously improve the survival rate of the mouse groups with lung metastasis. Notingly, although oral administered TFENs showed less accumulation amounts in the lungs with metastatic breast tumors than that *via* i.v. injection (Fig. 6M), the TFEN-treated group (i.v., high) and the TFEN-treated group (oral, high) achieved comparable reduced mortality rate and increased survival rate. These results can be ascribed to the fact that TFENs can exert the direct impacts on the proliferation, apoptosis, and mobility of cancer cells (Figs. 3 and 4) and also modulate the balance of intestinal microbiota (Fig. 6F–I).

### 3.7. *Biosafety evaluation*

To evaluate the pharmaco-toxicological characteristics of TFENs, we analyzed the changes of physiological and biochemical parameters in the TFEN-treated mice, including body weight variations, organ coefficients, immune system responses (pro-inflammation factors and complement C3), routine blood test, hepatorenal toxicity, and H&E staining of the major organs.

We found that no obvious variations in mouse body weights (Fig. 7A) and the main pro-inflammatory cytokines (Fig. 7B) were detected after repeated administration of high doses of TFENs. However, the TFEN-treated group (i.v., high) showed much heavier liver and spleen, in comparison with the control group and the TFEN-treated group (oral, high) (Fig. 7C). Moreover, the complement C3 concentrations in the TFEN-treated group (i.v., high) were significantly higher than those in the control group, while the TFEN-treated group (oral, high) had the similar level of complement C3 as the control group, demonstrating that TFENs could activate the complement system after i.v. injection (Fig. 7D). These results reflect that the surface contents (proteins, polysaccharides, and lipids) of TFENs after i.v. injection is likely to be treated as antigens by the immune system and trigger strong immune responses, while these contents might be degraded in the GIT, reducing their immunogenicity.

Blood compatibility is an essential requirement for biomedical application of TFENs *via* i.v. injection. Initially, a hemolysis assay was carried out to study the hemolytic property of TFENs, and these TFENs could not induce hemolytic phenomenon (Supporting Information Fig. S15). Furthermore, we examined the hepatorenal toxicities, as summarized in Fig. 7E–I. The concentrations of alanine aminotransferase (ALT), and aspartate aminotransferase (AST) in the blood from the TFEN-treated group (i.v., high) were significantly higher than those from the control group and the TFEN-treated group (oral, high), revealing the potential hepatotoxicity of TFENs after i.v. injection. Strikingly, all the blood parameters relevant to hepatorenal toxicities (Fig. 7E–I) and routine hemogram (Supporting Information Table S3) presented negligible statistical significance between the control group and the TFEN-treated group (oral, high). In addition, we found no obvious signs of tissue impairments in the major organs (heart, liver, spleen, lung, and kidney) and GIT from all the mouse groups (Fig. 7J and Supporting Information Fig. S16). Overall, intravenously injected TFENs can stimulate the activation of immune system, induce hepatorenal toxicities, and change the hemogram, while repeated administration of TFENs *via* oral route appear relatively safe for organisms.

## 4. Discussion

To date, large amounts of artificial nanotherapeutics have been demonstrated to be effective in the treatment of metastatic breast cancer[49,50]. However, few of them have been approved by regulatory agencies for clinic applications, which are ascribed to their limited therapeutic outcomes, potential adverse effects, and difficulty of large-scale production[51,52]. In the aspect of medical translation purpose, edible plant-derived nanovesicles have been proven as safe, inexpensive, and multi-functional platforms, in comparison with artificial nanotherapeutics[53]. Recently, natural exosome-like NPs have been extracted from several edible plants (*e.g.*, ginger, grapefruit, and citrus lemon) in large quantities. These nanotherapeutics have shown therapeutic effects in colitis, brain inflammatory diseases, and alcohol-induced liver damage[14]. However, there are lacks of roles in the treatment of metastatic cancers.

As reported, phytochemicals from edible plants could specifically exert their functions on tumor cells without affecting

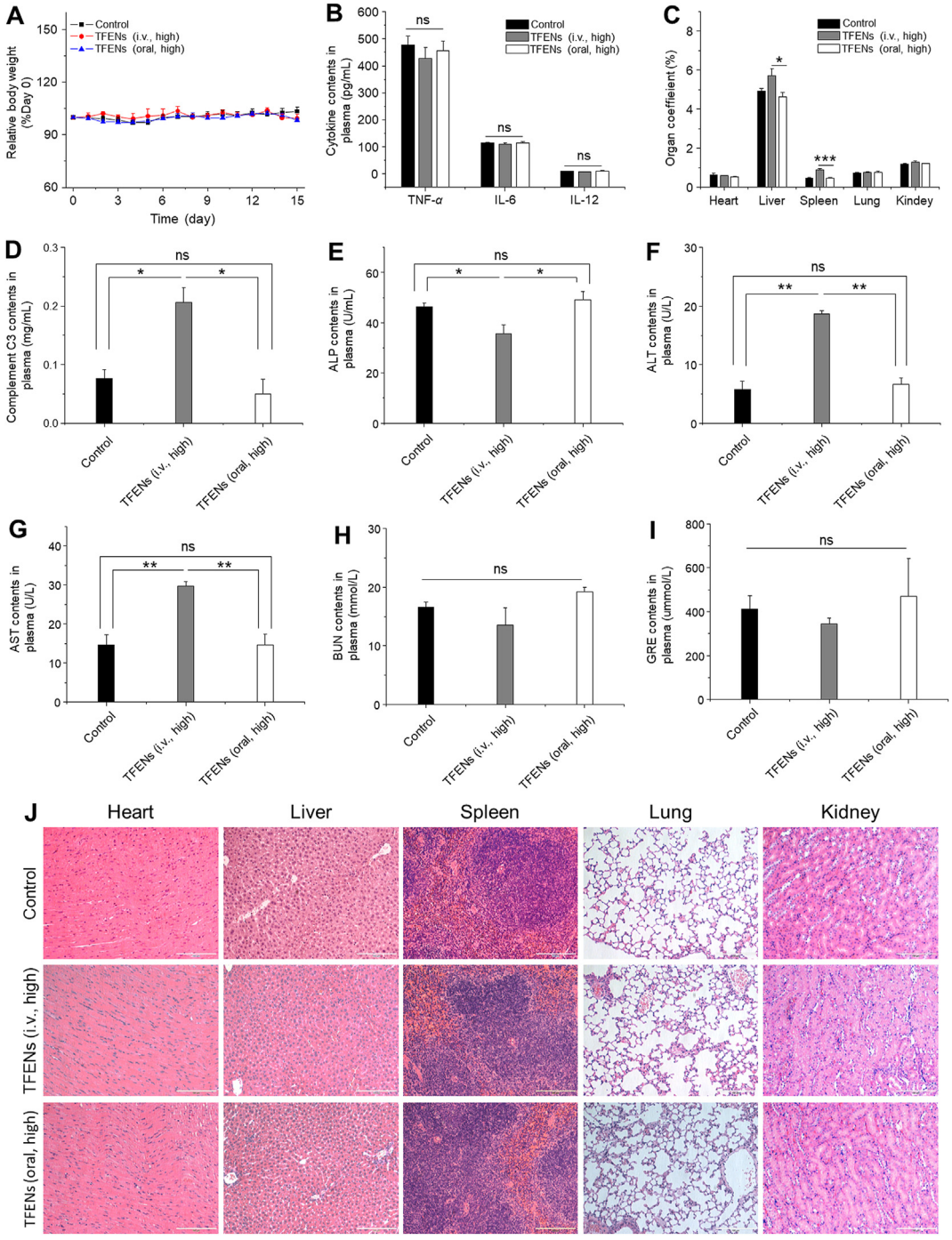


**Figure 7** *In vivo* biosafety evaluation of different treatment approaches. (A) Body weight variations (B) pro-inflammatory cytokine levels (C) organ coefficients (D) complement C3 (E) ALP (F) ALT (G) AST (H) BUN, and (I) GRE in plasma collected from the mice with the treatment of TFENs *via* i.v. and oral routes. (J) Histological analysis of the five main organs from the mice with the treatment of TFENs *via* i.v. and oral routes (scale bar = 100 μm). Each point represents the mean ± SEM ($n = 3$). *$P < 0.05$, **$P < 0.01$. ns, no significance.

normal cells[54]. In the present study, we hypothesize that tea flower-derived nanovesicles, containing large amounts of phytochemicals, can be used for the treatment of metastatic cancer. Since the physicochemical properties (*e.g.*, particle size, PDI, and zeta potential) of nanotherapeutics play important roles in determining their cellular uptake profiles, biodistributions, and therapeutic effects, these parameters are assessed. Unlike the particle sizes and surface charges of artificial NPs that can be easily modulated, these parameters of plant-derived nanovesicles mainly depend on plant resources. It was found that the TFENs with negative surface charges had particle sizes around 130 nm (Fig. 1C). These NPs were found to contain a large amount of polyphenols and flavonoids (Fig. 1G and H), which could interfere with various signaling pathways involving apoptosis, migration, and immune responses.

Subsequently, we demonstrated that TFENs could be internalized by cancer cells with high efficiency. It was reported that after co-incubation for 12 h, ginger-derived NPs were internalized

by 50% of 4T1 cells, and the uptake peak of these NPs by 4T1 cells was between 12 and 24 h[55]. In this study, the cellular uptake percentages of TFENs by 4T1 cells and MCF-7 cells were respective 57.2% and 94.6% after 5 h of incubation (Fig. 2B). The higher cell internalization rate of TFENs might be attributed to their surface contents, which could mediate the specific interaction with breast tumor cells.

The *in vivo* experiments revealed that TFENs could efficiently retard the growth and metastasis of breast tumors (Figs. 5 and 6). It was worth noting that orally administered TFENs achieved comparable therapeutic effects with TFENs *via* intravenous injection. These findings indicated that these NPs after oral administration could pass through the harsh gastrointestinal environment and be absorbed into circulatory system (Figs. 2E, 5A and 6A). A couple of studies have reported that plant-derived NPs were stable in the GIT, and their biological benefits provided a new perspective to understand cross-kingdom communications[56,57]. Also, we revealed the anti-cancer mechanism of TFENs, and their pro-apoptotic capacity was mainly dependent on the induction of increased oxidative stress in breast tumor cells (Fig. 4A). On the contrary, TFENs could induce few ROS production and weak mitochondria damage a in normal cell (HUVEC, Fig. S8). The high levels of oxidative stress triggered mitochondrial damage and cell cycle arrest, and two different patterns of cell cycle arrests were detected in MCF-7 cells and 4T1 cells (Fig. 4D and E). The binding of CYCLIN B to CYCLIN-dependent kinase (CDK1) would obtain the activated CDK1-CYCLIN B complex, which is pivotal in governing the progression of cell cycle from G2 to M phase[58]. The treatment of TFENs down-regulated the expression levels of CYCLIN B in MCF-7 cells, triggering the cell cycle arrest in the G2 phase. Nevertheless, the DNA can be damaged by the dramatically increased oxidative stress after the treatment of TFENs. In terms of 4T1 cells, the treatment of TFENs inhibited the cell cycle progression from S to G2 (S/G2). As reported, the CDK-CYCLIN A complex is critical for the transition of S/G2 phase[59], and our data suggests that the down-regulation of CYCLIN A can impair this transition, maintaining these cells in S/G2 phase. In addition to the outstanding treatment outcomes of TFENs, the anti-metastasis effect of TFENs was found (Fig. 6). Ki67 is known as a promising marker in predicting the recurrence risk. It was reported that patients with lower Ki67 index (less than 15%) had a lower recurrence rate and significantly better overall survival rate than those with higher Ki67 index[60,61]. Our data showed that the TFEN treatment groups had lower Ki67 levels, proving that TFEN treatments could inhibit tumor relapse. In addition, we found that oral administration resulted in less accumulation amounts of TFENs in the lungs than i.v. injection. However, both TFEN treatment groups *via* i.v. and oral routes achieved comparable increased survival rate (Fig. 6M), which could be attributed to the beneficial effects of oral administered TFENs on intestinal microbiota (Fig. 6F–I).

## 5. Conclusions

Tea flower-derived exosome-like nanoparticles (TFENs) were greenly produced by centrifugation and gradient ultracentrifugation. It was found that TFENs were enriched in various bioactive contents, including polyphenols, functional proteins, and lipids. The combined effects of these bioactive molecules triggered high oxidative stress in cancer cells, resulting in mitochondrial damage, cell cycle arrest, and the subsequent cell apoptosis. Further *in vivo* experiments revealed that TFENs preferentially accumulated in the breast tumor tissues and their lung metastatic sites, and the released bioactive contents could inhibit the growth of breast tumors and their lung metastasis through reactive oxygen species generation and microbiota modulation. This study contributes to the development of a robust 'green' nanotherapeutic for the treatment of metastatic breast cancer *via* oral route or intravenous injection, and this nanotherapeutic has a great potential for clinical translation.

## Acknowledgments

This work was supported by the National Natural Science Foundation of China (82072060 and 81571807, China), the Fundamental Research Funds for the Central Universities (XDJK2019TY002 and 2020CDJQY-A041, China), the Natural Science Foundation Project of Chongqing (cstc2020jcyj-msxmX0292, China), and the Venture & Innovation Support Program for Chongqing Overseas Returnees (cx2018029, China).

## Author contributions

Qiubing Chen and Qian Li contributed equally as joint first authors. Bo Xiao designed experiments, supervised studies, and wrote the manuscript. Qiubing Chen, Qian Li, Yuqi Liang, Menghang Zu, Nanxi Chen, Brandon S.B. Canup, and Liyong Luo performed the experiments. Chenhui Wang, Liang Zeng, and Bo Xiao edited and revised the manuscript. All authors have given approval to the final version of the manuscript.

## Conflicts of interest

The authors have no conflicts of interest to declare.

## Appendix A. Supporting information

Supporting data to this article can be found online at https://doi.org/10.1016/j.apsb.2021.08.016.

## References

1. Tang Y, Wang Y, Kiani MF, Wang B. Classification, treatment strategy, and associated drug resistance in breast cancer. *Clin Breast Cancer* 2016;**16**:335–43.
2. Kodack DP, Askoxylakis V, Ferraro GB, Fukumura D, Jain RK. Emerging strategies for treating brain metastases from breast cancer. *Cancer Cell* 2015;**27**:163–75.
3. Xiao Y, Cong M, Li J, He D, Wu Q, Tian P, et al. Cathepsin C promotes breast cancer lung metastasis by modulating neutrophil infiltration and neutrophil extracellular trap formation. *Cancer Cell* 2021;**39**:423–437 e7.
4. Poonia N, Lather V, Pandita D. Mesoporous silica nanoparticles: a smart nanosystem for management of breast cancer. *Drug Discov Today* 2018;**23**:315–32.
5. Panagi M, Voutouri C, Mpekris F, Papageorgis P, Martin MR, Martin JD, et al. TGF-beta inhibition combined with cytotoxic nanomedicine normalizes triple negative breast cancer microenvironment towards anti-tumor immunity. *Theranostics* 2020;**10**:1910–22.
6. Panagi M, Fojo T, Chamberlain C, Davis C, Sullivan R. Do patient access schemes for high-cost cancer drugs deliver value to society? Lessons from the NHS Cancer Drugs Fund. *Ann Oncol* 2017;**28**:1738–50.

7. Wortzel I, Dror S, Kenific CM, Lyden D. Exosome-mediated metastasis: communication from a distance. *Dev Cell* 2019;**49**:347−60.
8. Dai J, Su YZ, Zhong SY, Cong L, Liu B, Yang JJ, et al. Exosomes: key players in cancer and potential therapeutic strategy. *Signal Transduct Target Ther* 2020;**5**:145.
9. He CJ, Zheng S, Luo Y, Wang B. Exosome theranostics: biology and translational medicine. *Theranostics* 2018;**8**:237−55.
10. Jung KO, Jo H, Yu JH, Gambhir SS, Pratx G. Development and MPI tracking of novel hypoxia-targeted theranostic exosomes. *Biomaterials* 2018;**177**:139−48.
11. Li WY, Liu YS, Zhang P, Tang YM, Zhou M, Jiang WR, et al. Tissue-engineered bone immobilized with human adipose stem cells-derived exosomes promotes bone regeneration. *ACS Appl Mater Interfaces* 2018;**10**:5240−54.
12. Wu M, Ouyang Y, Wang Z, Zhang R, Huang PH, Chen C, et al. Isolation of exosomes from whole blood by integrating acoustics and microfluidics. *Proc Natl Acad Sci U S A* 2017;**114**:10584−9.
13. Sundaram K, Miller DP, Kumar A, Teng Y, Sayed M, Mu J, et al. Plant-derived exosomal nanoparticles inhibit pathogenicity of porphyromonas gingivalis. *iScience* 2019;**21**:308−27.
14. Iravani S, Varma RS. Plant-derived edible nanoparticles and miRNAs: emerging frontier for therapeutics and targeted drug-delivery. *ACS Sustainable Chem Eng* 2019;**7**:8055−69.
15. Teng Y, Ren Y, Sayed M, Hu X, Lei C, Kumar A, et al. Plant-derived exosomal microRNAs shape the gut microbiota. *Cell Host Microbe* 2018;**24**:637−652 e8.
16. Zhang MZ, Viennois E, Prasad M, Zhang YC, Wang LX, Zhang Z, et al. Edible ginger-derived nanoparticles: a novel therapeutic approach for the prevention and treatment of inflammatory bowel disease and colitis-associated cancer. *Biomaterials* 2016;**101**:321−40.
17. Raimondo S, Naselli F, Fontana S, Monteleone F, Lo Dico A, Saieva L, et al. Citrus limon-derived nanovesicles inhibit cancer cell proliferation and suppress CML xenograft growth by inducing TRAIL-mediated cell death. *Oncotarget* 2015;**6**:19514−27.
18. Chen D, Chen G, Chen C, Zeng X, Ye H. Prebiotics effects *in vitro* of polysaccharides from tea flowers on gut microbiota of healthy persons and patients with inflammatory bowel disease. *Int J Biol Macromol* 2020;**158**:968−76.
19. Liu LQ, Nie SP, Shen MY, Hu JL, Yu Q, Gong D, et al. Tea polysaccharides inhibit colitis-associated colorectal cancer *via* interleukin-6/stat 3 pathway. *J Agric Food Chem* 2018;**66**:4384−93.
20. Wang Y, Xia C, Chen L, Chen YC, Tu Y. Saponins extracted from tea (*Camellia sinensis*) flowers induces autophagy in ovarian cancer cells. *Molecules* 2020;**25**:5254.
21. Liu Y, Wu S, Koo Y, Yang A, Dai Y, Khant H, et al. Characterization of and isolation methods for plant leaf nanovesicles and small extracellular vesicles. *Nanomedicine* 2020;**29**:102271.
22. Zhang MZ, Xiao B, Wang H, Han MK, Zhang Z, Viennois E, et al. Edible ginger-derived nano-lipids loaded with doxorubicin as a novel drug-delivery approach for colon cancer therapy. *Mol Ther* 2016;**24**:1783−96.
23. Xiao B, Viennois E, Chen QB, Wang LX, Han MK, Zhang YC, et al. Silencing of intestinal glycoprotein CD98 by orally targeted nanoparticles enhances chemosensitization of colon cancer. *ACS Nano* 2018;**12**:5253−65.
24. Zheng MY, Xia QL, Lu SM. Study on drying methods and their influences on effective components of loquat flower tea. *LWT - Food Sci Technol (Lebensmittel-Wissenschaft -Technol)* 2015;**63**:14−20.
25. Way TD, Lin HY, Hua KT, Lee JC, Li WH, Lee MR, et al. Beneficial effects of different tea flowers against human breast cancer MCF-7 cells. *Food Chem* 2009;**114**:1231−6.
26. Li B, Jin YX, Xu Y, Wu YY, Xu JY, Tu YY. Safety evaluation of tea (*Camellia sinensis* (L.) O. Kuntze) flower extract: assessment of mutagenicity, and acute and subchronic toxicity in rats. *J Ethnopharmacol* 2011;**133**:583−90.
27. Koren E, Apte A, Jani A, Torchilin VP. Multifunctional PEGylated 2C5-immunoliposomes containing pH-sensitive bonds and TAT peptide for enhanced tumor cell internalization and cytotoxicity. *J Control Release* 2012;**160**:264−73.
28. Duan B, Zou S, Sun Y, Xu X. Fabrication of tumor-targeting composites based on the triple helical beta-glucan through conjugation of aptamer. *Carbohydr Polym* 2021;**254**:117476.
29. Xiao B, Merlin D. Oral colon-specific therapeutic approaches toward treatment of inflammatory bowel disease. *Expet Opin Drug Deliv* 2012;**9**:1393−407.
30. Huang Y, Canup BSB, Gou S, Chen N, Dai F, Xiao B, Li C. Oral nanotherapeutics with enhanced mucus penetration and ROS-responsive drug release capacities for delivery of curcumin to colitis tissues. *J Mater Chem B* 2021;**9**:1604−15.
31. Shan W, Zhu X, Liu M, Li L, Zhong JJ, Sun W, et al. Overcoming the diffusion barrier of mucus and absorption barrier of epithelium by self-assembled nanoparticles for oral delivery of insulin. *ACS Nano* 2015;**9**:2345−56.
32. Wang JJ, Zhu CG, Song D, Xia RQ, Yu WB, Dang YJ, et al. Epigallocatechin-3-gallate enhances ER stress-induced cancer cell apoptosis by directly targeting PARP16 activity. *Cell Death Dis* 2017;**3**:17034.
33. Chu KO, Chan KP, Yang YP, Qin YJ, Li WY, Chan SO, et al. Effects of EGCG content in green tea extract on pharmacokinetics, oxidative status and expression of inflammatory and apoptotic genes in the rat ocular tissues. *J Nutr Biochem* 2015;**26**:1357−67.
34. Li Y, Tang JL, Pan DX, Sun LD, Chen CY, Liu Y, et al. A versatile imaging and therapeutic platform based on dual-band luminescent lanthanide nanoparticles toward tumor metastasis inhibition. *ACS Nano* 2016;**10**:2766−73.
35. Stepanic V, Gasparovic AC, Troselj KG, Amic D, Zarkovic N. Selected attributes of polyphenols in targeting oxidative stress in cancer. *Curr Top Med Chem* 2015;**15**:496−509.
36. Batra P, Sharma AK. Anti-cancer potential of flavonoids: recent trends and future perspectives. *3 Biotech* 2013;**3**:439−59.
37. Zeeshan M, Murugadas A, Ghaskadbi S, Ramaswamy BR, Akbarsha MA. Ecotoxicological assessment of cobalt using Hydra model: ROS, oxidative stress, DNA damage, cell cycle arrest, and apoptosis as mechanisms of toxicity. *Environ Pollut* 2017;**224**:54−69.
38. Rogers C, Erkes DA, Nardone A, Aplin AE, Fernandes-Alnemri T, Alnemri ES. Gasdermin pores permeabilize mitochondria to augment caspase-3 activation during apoptosis and inflammasome activation. *Nat Commun* 2019;**10**:1689.
39. Green DR, Reed JC. Mitochondria and apoptosis. *Science* 1998;**281**:1309−12.
40. Cao HQ, Dan ZL, He XY, Zhang ZW, Yu HJ, Yin Q, et al. Liposomes coated with isolated macrophage membrane can target lung metastasis of breast cancer. *ACS Nano* 2016;**10**:7738−48.
41. Nilsson A, Johansson-Boll E, Sandberg J, Bjorck I. Gut microbiota mediated benefits of barley kernel products on metabolism, gut hormones, and inflammatory markers as affected by co-ingestion of commercially available probiotics: a randomized controlled study in healthy subjects. *Clin Nutr Espen* 2016;**15**:49−56.
42. Farzi A, Frohlich EE, Holzer P. Gut microbiota and the neuroendocrine system. *Neurotherapeutics* 2018;**15**:5−22.
43. Gomes AC, Hoffmann C, Mota JF. The human gut microbiota: metabolism and perspective in obesity. *Gut Microb* 2018;**9**:308−25.
44. Roy S, Trinchieri G. Microbiota: a key orchestrator of cancer therapy. *Nat Rev Cancer* 2017;**17**:271−85.
45. Alexander JL, Wilson ID, Teare J, Marchesi JR, Nicholson JK, Kinross JM. Gut microbiota modulation of chemotherapy efficacy and toxicity. *Nat Rev Gastroenterol Hepatol* 2017;**14**:356−65.
46. Rosean CB, Bostic RR, Ferey JCM, Feng TY, Azar FN, Tung KS, et al. Preexisting commensal dysbiosis is a host-intrinsic regulator of tissue inflammation and tumor cell dissemination in hormone receptor−positive breast cancer. *Cancer Res* 2019;**79**:3662−75.
47. Ingman WV. The gut microbiome: a new player in breast cancer metastasis. *Cancer Res* 2019;**79**:3539−41.

48. Marteau P. Bacterial flora in inflammatory bowel disease. *Dig Dis* 2009;**27**:99−103.
49. Chen QB, Ma Y, Bai P, Li Q, Canup BSB, Long DP, et al. Tumor microenvironment-responsive nanococktails for synergistic enhancement of cancer treatment *via* cascade reactions. *ACS Appl Mater Interfaces* 2021;**13**:4861−73.
50. Zhang XQ, Huang YM, Song HL, Canup BSB, Gou SQ, She ZG, et al. Inhibition of growth and lung metastasis of breast cancer by tumor-homing triple-bioresponsive nanotherapeutics. *J Control Release* 2020;**328**:454−69.
51. Dancy JG, Wadajkar AS, Connolly NP, Galisteo R, Ames HM, Peng S, et al. Decreased nonspecific adhesivity, receptor-targeted therapeutic nanoparticles for primary and metastatic breast cancer. *Sci Adv* 2020;**6**:eaax3931.
52. Landgraf M, Lahr CA, Kaur I, Shafiee A, Sanchez-Herrero A, Janowicz PW, et al. Targeted camptothecin delivery *via* silicon nanoparticles reduces breast cancer metastasis. *Biomaterials* 2020;**240**:119791.
53. Zhang M, Viennois E, Xu C, Merlin D. Plant derived edible nanoparticles as a new therapeutic approach against diseases. *Tissue Barriers* 2016;**4**:e1134415.
54. Tigu AB, Moldovan CS, Toma VA, Farcas AD, Mot AC, Jurj A, et al. Phytochemical analysis and *in vitro* effects of *Allium fistulosum* L. and *Allium sativum* L. extracts on human normal and tumor cell lines: a comparative study. *Molecules* 2021;**26**:574.
55. Wang Q, Zhuang X, Mu J, Deng ZB, Jiang H, Zhang L, et al. Delivery of therapeutic agents by nanoparticles made of grapefruit-derived lipids. *Nat Commun* 2013;**4**:1867.
56. Deng ZB, Rong Y, Teng Y, Mu JY, Zhuang XY, Tseng M, et al. Broccoli-derived nanoparticle inhibits mouse colitis by activating dendritic cell amp-activated protein kinase. *Mol Ther* 2017;**25**:1641−54.
57. Ju SW, Mu JY, Dokland T, Zhuang XY, Wang QL, Jiang H, et al. Grape exosome-like nanoparticles induce intestinal stem cells and protect mice from DSS-induced colitis. *Mol Ther* 2013;**21**:1345−57.
58. DiPaola RS. To arrest or not to G(2)-M cell-cycle arrest : commentary re: A. K. Tyagi et al., Silibinin strongly synergizes human prostate carcinoma DU145 cells to doxorubicin-induced growth inhibition, G(2)-M arrest, and apoptosis. *Clin Cancer Res* 2002;**8**:3311−4.
59. Bennin DA, Don ASA, Brake T, McKenzie JL, Rosenbaum H, Ortiz L, et al. CYCLIN G2 associates with protein phosphatase 2A catalytic and regulatory B′ subunits in active complexes and induces nuclear aberrations and a G(1)/S phase cell cycle arrest. *J Biol Chem* 2002;**277**:27449−67.
60. Soliman NA, Yussif SM. Ki-67 as a prognostic marker according to breast cancer molecular subtype. *Cancer Biol Med* 2016;**13**:496−504.
61. Paik S, Shak S, Tang G, Kim C, Baker J, Cronin M, et al. A multigene assay to predict recurrence of tamoxifen-treated, node-negative breast cancer. *N Engl J Med* 2004;**351**:2817−26.